Predictive Analog to Digital Conversion of Doppler Ultrasound Signals

Svein Bøe* and Kjell Kristoffersen†

Abstract — **Analog to digital conversion in multigate Doppler ultrasound systems for blood velocity measurements, is a technological challenge. The echoes must be digitized at a rate determined by the system bandwidth (typically 2 MHz), and the dynamic range is large (16 bits or more) due to the presence of strong, low-frequency Doppler clutter echoes originating from slowly moving tissue. Off-the-shelf A/D-converters do not meet these requirements with the transducer configuration employed by contemporary Doppler systems. Analysis reveals a 5 bits reduction in required wordlength for an A/D-converter in a predictive feedback loop, when the maximum clutter frequency is about 1.5 % of the pulse repetition frequency. The prediction error filter is recursive. Alternatively, first and second order DPCM (Differential Pulse Code Modulation) yield 4 and 6 bits respectively. With short input segments (from a high-resolution Color Flow Mapper), the results are, in the above order: 4, 4 and 5 bits. The results are verified by processing an experimental Doppler signal.**

I. Introduction

During the last decade, Doppler technology has become an important part of diagnostic ultrasound. In cardiac applications, blood velocity measurements using Spectral Doppler and/or Color Flow Mapping [1] are considered a standard part of an ultrasound examination.

A Color Flow Mapper transmits ultrasound pulses in various directions at a specified Pulse Repetition Frequency (PRF), typically in the kHz range. A number of consecutive pulses are fired in each direction before the beam angle is changed. Each reflected signal is passed through a complex demodulator and low-pass filter before the signals from one direction are handled by a multigate Doppler [2]–[4].

A multigate Doppler samples the low-pass filter output at a number of range gates. Each range gate is associated with a small sample volume at a corresponding depth. Conceptually, each sample volume is processed separately at a rate equal to the PRF, but in practice a single unit may operate serially on all the gates. There are thus two sampling rates involved: one is determined by the range gate spacing, the other is the PRF. To avoid range ambiguity, the PRF cannot be too high. On the other hand, the PRF should be high in order to avoid aliasing.

Sensitivity is a key issue in cardiac Doppler applications, particularly in cases where one wants to detect small, high-velocity jets at large ranges. When a large range and a high PRF implies range ambiguity, the primary range gate may be set close to zero range, corresponding to a time delay from one of the previous pulses (High-PRF pulsed Doppler, with deliberate use of range ambiguity to reduce aliasing-problems [5]). This requires a system with a large instantaneous dynamic range, because the echoes from tissue at a close range are extremely large. In Color Flow Mapping without range ambiguity, the dynamic range may be very large when the weak echoes from a small vessel are mixed with large tissue echoes. A typical signal bandwidth in Color Flow Mapping is 2 MHz, requiring a distance between sample volumes of 0.5 μs (0.375 mm). This may be a challenge for the A/D-converter (ADC), depending on the required dynamic range.

A. Required dynamic range

We estimate the required dynamic range by considering the fundamental system noise level compared with the large tissue echoes. The processing should increase the system noise level only by a negligible amount while at the same time not be saturated by the large echoes originating from tissue.

The system's fundamental noise level is determined by the thermal noise from the real part of the transducer's electrical impedance. Modern systems employ digital signal processing, and quantization noise from the ADC summed with electronic front-end noise determine the effective noise figure [6] of the system. Optimal sensitivity requires a noise figure close to unity, regardless of range. This demands a front-end with the largest instantaneous dynamic range possible.

In B-mode imaging, time gain compensation attenuation is used in the nearfield to get a signal depth-independent amplitude. However, gain reduction in the front-end of a system designed for a wide instantaneous dynamic range is associated with an increase in the noise figure. Time gain compensation must be minimized in our case.

Tissue moves much more slowly than blood, so these clutter echoes may be suppressed by high-pass filtering the signal at each range gate, thus reducing the signal's dynamic range (fixed target canceler or stationary canceler [7]). The high-pass filtering is normally performed after digitization of the signal [2], for increased flexibility.

The remaining question is how large instantaneous dynamic range is required, or, equivalently, how many bits are needed in the A/D-conversion (ADC) of the signal. The answer is "the more the better", since there will always be more diagnostic situations that can be covered with a larger dynamic range. For measurements with a low PRF at large ranges, a relatively small number of bits (say 8–10 bits/gate, depending on the bandwidth) may be sufficient, because the tissue echo from large depths is not very large. High PRF measurement of high-velocity jets at large ranges easily calls for a 16 bits digitization at a 2 MHz rate. Baseband processing brings the required sampling frequency down to 1 MHz for each chan-

*S. Bøe is with Department of Informatics, University of Oslo, P.O. Box 1080, N-0316 Oslo, Norway

†K. Kristoffersen is with Vingmed Sound AS, Research Department, Vollsveien 13C, N-1324 Lysaker, Norway

nel.

B. Possible solutions

Oversampling techniques [8], [9] for high-speed ADC do not make sense when each sample volume in a multigate Doppler is processed separately. The sampling frequency for each gate is fixed at the PRF, and non-oversampling ADCs cannot yet fulfill the requirements [10]–[12]. With serial processing, all the gates along an echo return signal may be handled by the same converter, which could be of the oversampling kind. Present technology provides devices which are close to meeting the requirements [13], but the cost of these may be prohibitive. In this paper, we have chosen a different route.

Non-uniform quantization [8] of the Doppler signal will not be successful because the quantization step size is increased with signal amplitude. A Doppler signal typically consists of a weak high-frequency blood Doppler component on top of a large low-frequency clutter component, and the large quantization intervals will not capture the fine detail.

It is apparent that cost-effective digitization is a challenge in the design of high-quality multigate Doppler systems. Brandestini [2] proposed to move the ADC within a feedback loop, so that it digitizes the difference between the present echo and a prediction formed on the basis of the previous echoes. Brandestini [2], [14, [15] and Hoeks [3], [4] analyzed a system with this "Brandestini loop" (Moving Target Indicator [7] or tracking ADC) and reported a gain of 2 bits of dynamic range [3].

Brandestini and Hoeks used the feedback loop as an active part of a fixed-target cancelling filter for attenuation of tissue echoes. This implies constraints on the prediction filter. Our objective is to identify a prediction filter with the smallest prediction error possible, without any predefined constraints on its frequency response, digitize that prediction error, and then add the error to the prediction to form the final output. The resulting converter will be called a Predictive ADC, and it will be thoroughly analyzed.

Predictive coders such as Differential Pulse Code Modulators (DPCMs) and Delta Modulators are well known [8], [16]. They are also used for ADC, and in this paper we will compare the "Brandestini loop", Predictive ADC and Differential Pulse Code Modulation (DPCM).

II. Signal Model and Conventional ADC

The signal return for one pulse can be written

$$\Re\{\tilde{s}_n(\tau)e^{j\,2\pi\,f_0\tau}\},$$

where $\Re$ means real part, n is the pulse number, f_0 is the carrier frequency, and $\tilde{s}_n(\tau)$ is the complex envelope. The contribution from a sample volume at a distance d from the transducer face, is represented by the sample taken at $\tau = 2d/c$, where τ is the elapsed time since the pulse was transmitted, and c is the velocity of sound in tissue. By sampling consecutive pulses after complex demodulation and low-pass filtering, the discrete-time signal

$$s[n] = \tilde{s}_n(2d/c) = x[n] + jy[n] \tag{1}$$

carries the information from a single sample volume, where x and y are the real and quadrature components respectively. The sampling frequency (f_s) in (1) equals the PRF. The digitization rate in a multigate Doppler with serial processing is much higher than the PRF.

The signal $s[n]$ is contaminated with white thermal noise from the transducer and the front-end. We assume independent quantization of the quadrature components. Each component is modeled as a sum of three signals,

$$x[n] = c[n] + b[n] + t[n],$$

where $c[n]$, $b[n]$ and $t[n]$ represent contributions from clutter, blood and thermal noise respectively.

A spectral model for $x[n]$ can be established by noting that tissue moves slower than blood, that the clutter-to-blood ratio can become very large, and that the blood-to-noise ratio is much smaller. A visual inspection of a signal spectrum estimate suggests that the clutter $c[n]$ may be modeled as a low-frequency rectangular spectrum. Blood and white noise are lumped into a common component $w[n]$, which is also considered white,

$$\begin{aligned} w[n] &= b[n] + t[n] \\ x[n] &= c[n] + w[n]. \end{aligned} \tag{2}$$

The lumping of $b[n]$ and $t[n]$ is based on the large difference in power density levels between clutter and any of $b[n]$ and $t[n]$. The assumption of whiteness relates to the situation where the signal from blood is about to drown in white noise and thus demands the greatest dynamic range.

The amplitude resolution required from an ADC may be determined from the noise power σ_w^2 of the system, while the number of bits is subsequently determined by the peak signal amplitude. The peak or instantaneous dynamic range prior to quantization is

$$\mathrm{DR}_{\mathrm{peak}} = \max|x[n]|/\sigma_w, \tag{3}$$

After quantization, $\mathrm{DR}_{\mathrm{peak}} = \max|x[n]|/(\sigma_w^2 + \sigma_{\mathrm{AD}}^2)^{1/2}$, where $\sigma_{\mathrm{AD}}^2 = \Delta^2/12$ [17] is the power of white, uniform probability density quantization noise with step size Δ. Quantization must not significantly increase the noise level. Allowing a $\mathrm{DR}_{\mathrm{peak}}$ reduction of about 1 dB we get

$$\sigma_{\mathrm{AD}}^2 \leq \sigma_w^2/4 \tag{4}$$

$$\Delta \leq \sigma_w\sqrt{3}. \tag{5}$$

The required number of levels in the ADC is

$$L_x = 2[\frac{\max|x[n]|}{\Delta}] + 1, \tag{6}$$

where $[x]$ is rounding, which will be omitted for notational simplicity. The word-length ($R_x = \lceil \log_2 L_x \rceil$, where $\lceil x \rceil$ is rounding upwards) of the ADC can be decreased if the signal peak is reduced.

The rectangular spectrum signal model is characterized by the maximum clutter frequency f_c and the instantaneous or peak Clutter to Noise Ratio (CNR)

$$\mathrm{CNR}_{\mathrm{peak}} = \max|c[n]|/\sigma_w. \tag{7}$$

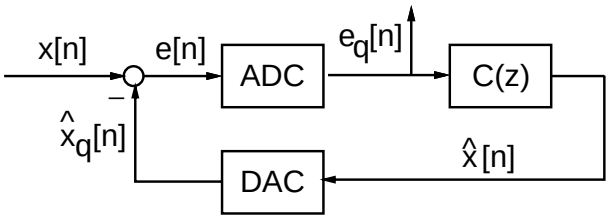

Fig. 1. "Brandestini loop" and basic component of a Predictive ADC with discrete-time signals. The signals $x[n]$ and $e[n]$ have continuous amplitude, the rest have quantized amplitudes, with $\hat{x}_q[n]$ coarser than $\hat{x}[n]$. The signal $\hat{x}[n]$ is a prediction of $x[n]$. The filter $\mathcal{C}(z)$ needs to be determined.

Inserting (5) with equality in (6) and using (3), the minimum number of levels is expressed in terms of these parameters,

$$L_x = \frac{2}{\sqrt{3}}\mathrm{DR}_{\mathrm{peak}} + 1 \approx \frac{2}{\sqrt{3}}\mathrm{CNR}_{\mathrm{peak}}, \tag{8}$$

where the approximation is valid for large $\mathrm{CNR}_{\mathrm{peak}}$ because of (7), (3) and (2).

The number of bits required to represent a signal with a large dynamic range and given noise level σ_w^2 without overloading the converter is thus dictated by $\mathrm{CNR}_{\mathrm{peak}}$.

III. Model of a Predictive ADC

One approach to reducing the peak dynamic range into the ADC is to subtract a model of the low-frequency clutter component from the observations prior to digitization.

A block-diagram of the "Brandestini loop" is shown in Fig. 1, with $\mathcal{C}(z)$ representing a filter which needs to be designed [2]–[4], [14, [15]. The feedback loop produces an error signal $e[n]$, which is the difference between the present input $x[n]$ and a prediction of the same, $\hat{x}_q[n]$. The error will typically have a smaller dynamic range and need fewer bits. In the figure, $x[n]$ is the echo return from a single sample volume in the body.

Fig. 1 has been analyzed in the context of a multigate Doppler for peripheral vessels [2–4], [14], [15]. The motivation was to decrease the word-length requirement on the ADC and to contribute to cancellation of low-frequency clutter. The error signal $e_q[n]$ was the output from the loop, and the filter between $x[n]$ and $e[n]$ was one stage of a high-pass filtering chain. Denoting the prediction error filter by $\mathcal{B}(z)$, its transfer function was [3]

$$\mathcal{B}(z) = \mathcal{E}(z)/\mathcal{X}(z) = \frac{1 - z^{-1}}{1 - az^{-1}}, \ |a| < 1, \tag{9}$$

with $a = 7/8$ or $a = 15/16$. The filter $\mathcal{C}(z)$ is

$$\mathcal{C}(z) = \hat{\mathcal{X}}(z)/\mathcal{E}(z) = \frac{(1-a)z^{-1}}{1 - z^{-1}}. \tag{10}$$

In the previous papers, the parameter a was restricted to give $\mathcal{B}(z)$ the desired high-pass frequency response, i.e. a was nonnegative and close to 1. This leads to a small cutoff-frequency, a steep transition around 0 Hz, and a rather flat response at higher frequencies, see Fig. 2.

Our motivation is restricted to word-length reduction. Clutter rejection will be handled by a different processing unit.

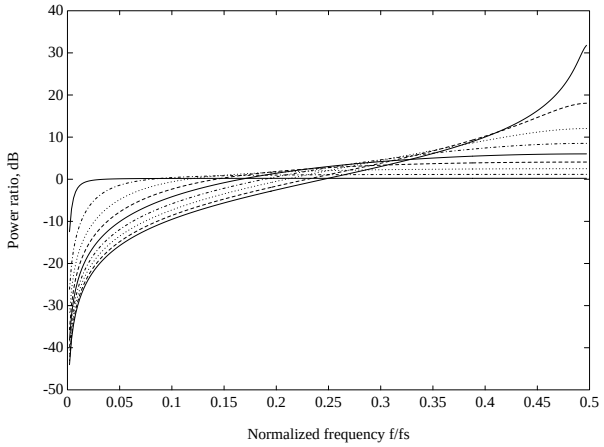

Fig. 2. Frequency response of prediction error filter $\mathcal{B}(z)$. Both the high-frequency boost and cutoff frequency increase as a approaches -1. Curves are shown for $a = \pm 0.95, \pm 0.75, \pm 0.5, \pm 0.25, 0.0$. Previous implementations have $a \approx 0.95$, with flat high-frequency response and low cutoff frequency.

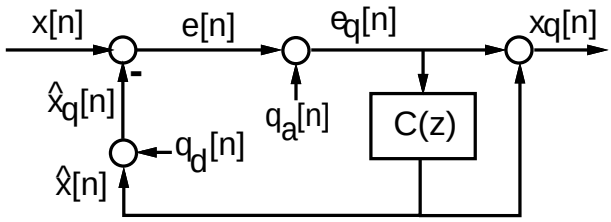

Fig. 3. Model of the Predictive ADC, including the generation of $x_q[n] = \hat{x}[n] + e_q[n]$. Quantization noises $q_a[n]$ and $q_d[n]$ represent the ADC and D/A-converter (DAC) respectively, and $q_d[n]$ is known.

The best approximation to $x[n]$ should be the loop output. The signal $\hat{x}[n] + e_q[n]$ is a natural candidate, because the transfer function between $x[n]$ and this signal is unity for all a. This gives more freedom in choosing a value for a, and it is the key to the improvements over the "Brandestini loop".

When the loop in Fig. 1 is modified to produce $x_q[n] = \hat{x}[n] + e_q[n]$, it will be termed a Predictive ADC. A model is shown in Fig. 3. It resembles a Differential Pulse Code Modulator (DPCM), and a comparison is found in Section V.

IV. Analysis of the Predictive ADC

In this section we develop an expression for the reduction in the number of bits necessary for the ADC.

A. Quantization noise

The total quantization noise introduced by the Predictive ADC should not be any larger than for a conventional ADC. For the latter, the restriction is given by (4). With the Predictive ADC in Fig. 3, the transfer function from $x[n]$ to $x_q[n]$ as well as those from $q_a[n]$ and $q_d[n]$ to $x_q[n]$ are unity, so neither the inherent noise in $x[n]$ nor the quantization noises are affected by the loop. There is no noise-shaping, in contrast to oversampling converters [9]. The quantization step size of the ADC in the loop, determined by the inherent noise power in the output signal $x_q[n]$, may thus be determined by the noise

power in $x[n]$. The step size is again given by (5). The error caused by the finite quantization step of the D/A-converter (DAC) is known, and can be corrected for. We therefore assume that the DAC does not contribute to the quantization noise.

B. Word-length reduction

The reduction in wordlength is ((6) with $\Delta \ll \max|x[n]|$ and $\Delta \ll \max|e[n]|$)

$$\delta R = \log_2 \frac{L_x}{L_e} = \log_2 \frac{\max|x[n]|}{\max|e[n]|}. \tag{11}$$

With $\max|x[n]| = \lambda_x \sigma_x$ and $\max|e[n]| = \lambda_e \sigma_e$, where λ_x and λ_e are loading factors [8], and the assumption $\lambda_x = \lambda_e$, the reduction is also

$$\delta R = \frac{1}{2} \log_2 \frac{\sigma_x^2}{\sigma_e^2}. \tag{12}$$

The expression in (11) is the important one in practice, but (12) is better suited for analysis. This power ratio or prediction gain will be analyzed.

It is customary to consider medical Doppler ultrasound signals as stationary over 10 ms intervals, because the velocity profile is essentially constant over such short segments. With this assumption for $x[n]$, $e[n]$, $c[n]$ and $w[n]$, and that the latter two are uncorrelated, we have from (2) and (9) that

$$P_e(f) = \frac{1}{T^2}(P_c(f) + P_w(f))|B(f)|^2, \tag{13}$$

where $P_c(f)$, $P_w(f)$ and $P_e(f)$ are power density spectra for the corresponding signals, $B(f) = T\mathcal{B}(e^{-j\,2\pi\,fTk})$, and $T = 1/\text{PRF}$ is included for proper scaling [18]. Exploiting the rectangular shape of the signal model and integrating (13), the prediction error power is

$$\begin{aligned} \sigma_e^2 &= (P_c + P_w) \int_{-f_c}^{f_c} \frac{1}{T^2} |B(f)|^2 \, df \\ &\quad + 2P_w \int_{f_c}^{f_s/2} \frac{1}{T^2} |B(f)|^2 \, df. \end{aligned} \tag{14}$$

With $\mathcal{B}(z)$ given by (9), the reciprocal of prediction gain is found in Appendix A for $a \in \langle -1, 1\rangle$, as a function of $\text{CNR}_{\text{rms}} = \sigma_c/\sigma_w$, a and f_c. The plot in Fig. 4 shows word-length reduction for $\text{CNR}_{\text{rms}} = 40$ dB (solid curves) and 90 dB (dashed curves) for four values of f_c. It is based on (12) and expression (A.5) from the appendix. In general, word-length reduction increases with decreasing clutter signal bandwidth, increasing prediction error filter high-frequency boost and cutoff frequency ((9) and Fig. 2 with decreasing a). This trend is reversed when a approaches -1 (especially when low-frequency clutter is combined with a relatively small CNR_{rms}). The reason for the unfavourable situation when $a \approx -1$ is that the high-frequency gain for $\mathcal{B}(z)$ (at $f = f_s/2$) approaches infinity when a approaches -1.

An approximation for word-length reduction is developed in Appendix A. The reduction is independent of CNR_{rms} above a threshold which increases with decreasing a and decreasing f_c. Below the threshold, word-length reduction increases with CNR_{rms}. This is displayed by the difference between solid and dashed curves in Fig. 4. The case with $\text{CNR}_{\text{rms}} = 90$ dB is a better reference for the large CNR_{peak} which may occur in practice, and an even larger CNR_{peak} would not alter the dashed curves.

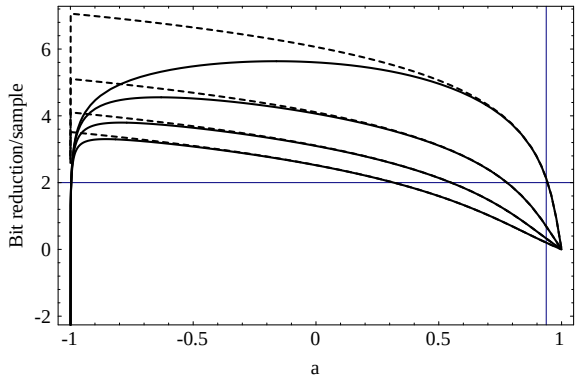

Fig. 4. Word-length reduction for $\text{CNR}_{\text{rms}} = 40$ dB (solid) and 90 dB (dashed) with $f_c = 0.048 f_s$ (bottom), $f_c = 0.032 f_s$, $f_c = 0.016 f_s$ and $f_c = 0.004125 f_s$ (top) as a function of filter parameter a. The cross-hair indicates previous results. See text.

With $e_q[n]$ as the loop output, the word-length reduction is only two bits [3]. In Hoeks' paper [3], $a = 15/16$ and $f_c = 0.004125 f_s$. Fig. 4, top solid and dashed curves, correspond in maximum clutter frequency. The cross-hair in the plot shows that the two bit reduction agrees well. The use of $x_q[n]$ as output along with a different choice of parameter a, relaxes the requirements on the ADC.

The reason why this paper comes up with better results is that by letting a approach -1, high gain at $f_s/2$ in $B(f)$ is introduced for an improved attenuation at 0 Hz, where most of the clutter power is concentrated. This gain was not desirable in previous designs, but in the present configuration there is no shaping of the output spectrum.

V. Differential Pulse Code Modulation (DPCM) versus Predictive ADC

A Differential Pulse Code Modulator (DPCM) with discrete-time input is shown in Fig. 5, with $x_q[n]$ representing the approximation to the input $x[n]$. The filter $\mathcal{D}(z)$ is an N'th-order Finite Impulse Response (FIR) prediction filter with coefficients $d_1, \ldots, d_N$. Redrawing the Predictive ADC from Fig. 3 with $\mathcal{C}(z)$ from (10) and quantization noise sequences replaced by an ADC and a DAC, we get Fig. 6. The solid lines show the "Brandestini loop", and the dashed lines show the generation of the Predictive ADC output. The new variable $\tilde{x}[n]$ is the output of a leaky integrator with input $x[n]$, $\tilde{\mathcal{X}}(z)/\mathcal{X}(z) = 1/(1 - az^{-1})$.

With $a = 0$, the Predictive ADC becomes a first order DPCM with a simple delay-predictor $\mathcal{D}(z) = z^{-1}$. Fig. 4 is thus also applicable for first order DPCM.

When used with a multigate Doppler, the Predictive ADC or the DPCM can be time-shared between different sample volumes. If the number of sample volumes is M, the only modification necessary, is to replace z^{-1} in $\mathcal{B}(z)$, $\mathcal{C}(z)$ and $\mathcal{D}(z)$ by z^{-M}.

Comparing the Predictive ADC with the DPCM, we find that both have unity overall transfer functions $\mathcal{X}_q(z)/\mathcal{X}(z) =$

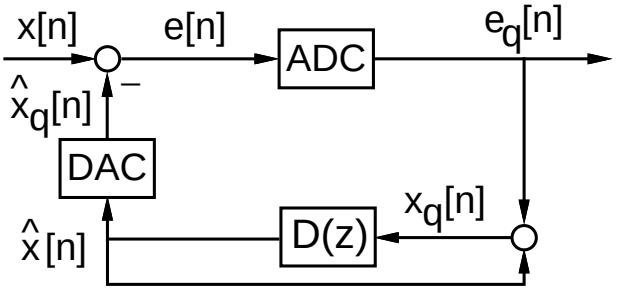

Fig. 5. Differential Pulse Code Modulator (DPCM). The filter $\mathcal{D}(z)$ is an N'th order FIR predictor.

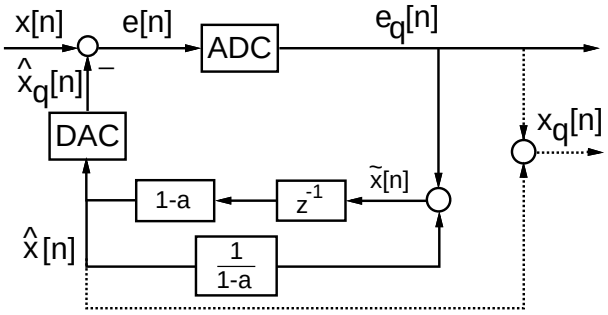

Fig. 6. Predictive ADC. The solid lines represent the "Brandestini loop", while the dashed lines represent the add-ons for a Predictive ADC. The unnecessarily complicated appearance is chosen for ease of comparison with Fig. 5.

1 (the quantization noises are not shaped). The filter $\mathcal{C}(z)$ between $e[n]$ and $\hat{x}[n]$ is given by (10) for the Predictive ADC and

$$\mathcal{C}(z) = \frac{\hat{\mathcal{X}}(z)}{\mathcal{E}(z)} = \frac{\mathcal{D}(z)}{1-\mathcal{D}(z)} \tag{15}$$

for the DPCM. Both are error-accumulating Infinite Impulse Response (IIR) filters. The prediction error filter between $x[n]$ and $e[n]$ is an FIR filter in the DPCM case,

$$\mathcal{B}(z) = \frac{\mathcal{E}(z)}{\mathcal{X}(z)} = 1-\mathcal{D}(z), \tag{16}$$

whereas the Predictive ADC uses the IIR filter in (9). Between the error $e[n]$ and the final output $x_q[n]$, both cases use IIR filters,

$$\frac{\mathcal{X}_q(z)}{\mathcal{E}(z)} = \begin{cases} \dfrac{1}{1-\mathcal{D}(z)}, & \text{DPCM} \\ \dfrac{1-az^{-1}}{1-z^{-1}}, & \text{Predictive ADC.} \end{cases} \tag{17}$$

An approximation for the performance of DPCM is given by the prediction gain σ_x^2/σ_e^2 at the different predictor orders [8], [16]. The maximum obtainable gain is the reciprocal of the spectral flatness γ_x^2 of the input signal,

$$\gamma_x^2 = \frac{1}{\sigma_x^2}\exp\left\{\int_{-1/2}^{1/2}\log_e P_x(f)df\right\}. \tag{18}$$

The prediction gain often saturates for low order predictors.

TABLE I

MAXIMUM DURATION n_0 OF INITIAL TRANSIENT (FOR A STEP INPUT, $R_x = 11$ AND WORD-LENGTH R_e, SECTION VI), AND WORD-LENGTH REDUCTION δR (DISREGARDING INITIAL TRANSIENTS, SUBSECTION VIII.B). THE RESULTS ON n_0 FOR SECOND ORDER DPCM COME FROM SIMULATIONS (SUBSECTION VIII.C). THE PARAMETER VALUES ARE DETERMINED IN SECTION VIII.

Method	Parameter	R_e	n_0	δR
PADC	$a = -0.95$	6	1*	5†
DPCM	$d_1 = 0.9987$	7	1	4
	$d_1 = 1.967$	5	2*	6†
	$d_2 = -0.9697$	6	1*	5†

*Increased by at least 1 for 12-sample input segments from the wall thump region in Fig. 7, when R_e is unchanged. See Subsection VIII.C.

†Must be reduced by 1 for 12-sample input segments from the wall thump region in Fig. 7, when n_0 is required not to change. Correspondingly, R_e is increased by 1. See Subsection VIII.C.

VI. INITIAL TRANSIENT OF CLOSED LOOP ADC

Saturation of the ADC is especially likely to occur for a large initial input sample because $e[0] = x[0]$, for the Predictive ADC as well as for the DPCMs. Overloading will change the future samples of $e[n]$, and an initial transient will appear in the final output $x_q[n]$. We will use a step input to analyze the duration of the initial transient. It is defined as the number of samples before the absolute error of the output $x_q[n]$ becomes smaller than $\Delta/2$ (equivalent to the number of overloading samples). Proper initialization may shorten the transient. This is especially important for Color Flow Mapping, which may use signal segments of only 8–10 samples. We treat the initialization problem for each sample volume separately.

One possibility for initialization is to use a converter with a larger step size for the first sample. An ADC with adjustable gain could provide two different step sizes and eliminate the need for a second converter. The coarse step will be chosen to avoid overload for the first sample. The maximum duration of the Predictive ADC and first order DPCM ($a = 0$) transient is (Appendix B),

$$n_0 \approx \lceil \frac{2^{R_x-2R_e} - 1 + 2^{-R_e}}{1-a} \rceil + 1$$

samples, where R_e is the reduced ADC word-length. Results for Predictive ADC and first order DPCM are given in Table I, with $R_x = 11$ determined in Section VIII. For second order DPCM we rely on simulations (Subsection VIII.C).

VII. SENSITIVITY ANALYSIS

Errors may occur in the ADC, subtraction and DAC gain (the latter two arise in the same component, a difference amplifier). They may lead to an overloaded ADC which may be a symptom of an increased transient duration or of an increased dynamic range for $e[n]$. The accumulated effect of the errors are analyzed by including a constant gain factor other than unity and a constant offset error in the DAC output. The maximum allowable increase in dynamic range is set to 0.5 bit, and the transient duration is not allowed to exceed the results

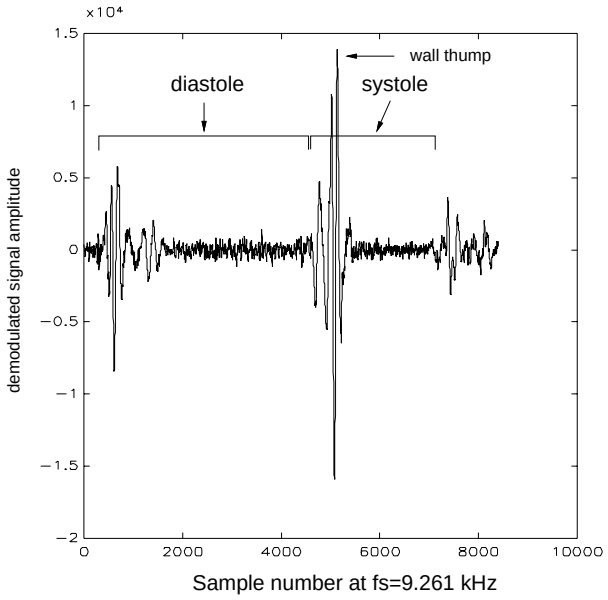

Fig. 7. Experimental echo signal from the aorta, taken from the output of the lowpass filter in the quadrature demodulator.

from the error-less case with initialization.

Appendix C shows that a gain error of $|\delta g| = |1-g| \leq 2$ % will satisfy the requirements on dynamic range and transient duration for Predictive ADC and first order DPCM with the parameters listed in Table I. A 2 % error is well within available component tolerances. The requirement on transient duration is satisfied for second order DPCM with $R_e = 6$. Further results are given from simulations in Subsection VIII.D.

The offset error is automatically compensated for in $\hat{x}[n]$, unless the digital filter registers are limited. It will not by itself cause any problems. The effect when combined with a gain error has been simulated in Subsection VIII.D.

VIII. Simulated Performance

A signal collected from a Doppler instrument was used to verify the theoretical results. Maximum clutter frequency f_c, CNR_{peak} and spectral flatness must be determined. The signal segments containing echoes from tissue represent the largest dynamic range and the largest potential for word-length reduction. The following results appear from analysis of signal sections corresponding to a wall thump.

A. Experimental signal

The experimental signal comes from measurements of blood flow in the aorta using a modified Vingmed "Alfred"[1] pulsed wave single-gate Doppler instrument. The signal was acquired from one of the low-pass outputs of the quadrature demodulator in the instrument. The carrier frequency was 2 MHz, the PRF was 9.26 kHz, and the signal was sampled with a high-resolution (16 bits) ADC. Fig. 7 shows a section of 8400 samples (0.9 seconds) from the signal.

The maximum equivalent mean-square bandwidth estimate [18], for segments of the signal, gives $\hat{f}_c = 0.016 f_s = 148$ Hz for sliding Welch spectrum estimates with Hanning data-window and 8.6 ms equivalent segment duration [18].

[1] Manufactured by Vingmed Sound AS

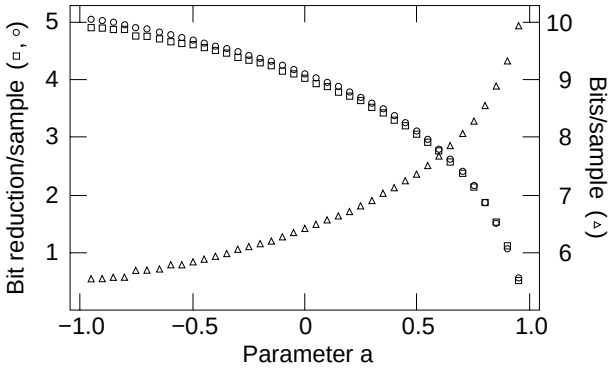

Fig. 8. Estimated word-length reduction δR (left axis) with a Predictive ADC for the wall thump samples in Fig. 7 ('○' for analytical results, '□' for filtering without quantization and initial transients). Minimum word-length R_e for the ADC in the Predictive ADC loop ('△', right axis), without initial transient, according to simulations. $R_x = R_e + \delta R = 11$ bits, and a was varied in steps of 0.05.

With $\text{CNR}_{\text{peak}} \approx \text{DR}_{\text{peak}}$, we have from (3) that the estimated CNR_{peak} is 62 dB, where σ_w is estimated with a Welch periodogram in late diastole (where the blood Doppler component is very small). Using this in (8) requires $R_x = 10.4 \rightarrow 11$ bits for conventional ADC, equivalent to dividing DR_{peak} by 6 (dB/bit).

The spectral flatness in (18) of the rectangular-model signal with $f_c = 0.016 f_s$ and $\text{CNR}_{\text{peak}} = 62$ dB is -59 dB.

B. Word-length reduction

Predictive ADC: Estimates of Predictive ADC word-length reduction are shown in Fig. 8 along the left vertical axis. The '□' symbols come from filtering the experimental signal with the prediction error filter $\mathcal{B}(z)$ and using (11), without quantization and after removal of the initial transient. The parameter a was varied in steps of 0.05. The data-set labelled '○' comes from the analytical result in (12) and (A.5) for the signal model, using $\hat{f}_c$ Hz and $\text{CNR}_{\text{rms}} = \text{DR}_{\text{peak}}$. The maximum word-length reduction is 5 bits when $a = -0.95$ (among the chosen values for a). A value which would speed up implementations, is $a = -15/16 = -0.9375$, and the change in performance is negligible. Compared with Fig. 4 we see that the case with $\text{CNR}_{\text{rms}} = 90$ dB is a good approximation.

An expected minimum word-length for the experimental signal wall thump segment becomes $R_e = R_x - 5 = 6$ bits.

The Predictive ADC was simulated with quantization. The signal in Fig. 7 was used as input, and (6) was applied to the error to find L_e and the word-length R_e. Results are shown in Fig. 8 ('△' along the right vertical axis) as the required number of bits for $e[n]$ without overloading the ADC. One can get by with 6 bits word-length, as expected.

DPCM: The filter coefficient for first order DPCM was estimated with a first-order AR-model using the modified-covariance algorithm [18], [19] on the wall thump segment. Estimating the word-length by first applying the corresponding prediction error filter gives $\delta R = 4.0$ bits and $R_e = 6.4 \rightarrow 7$ bits. A second order predictor based on a second order AR-model gives $\delta R = 5.8$ bits and $R_e = 4.5 \rightarrow 5$ bits. Simu-

lations with quantization gave the same results within 0.1 bit, after exclusion of the initial transient. A tenth order predictor only gained an additional 0.4 bit. The main results are summarized in Table I.

C. Initial transients

For the Predictive ADC and first order DPCM, the results on the duration of the initial transient for a step input in Section VI and Table I, were confirmed with simulations. For second order DPCM, we used the AR parameters from fitting to the wall thump segment (which is also rather lowpass) when processing the step input. With $R_e = 5$ and 6, the results were $n_0 = 2$ and 1 samples respectively.

Simulations were run with 12-sample segments from the signal in Fig. 7 as loop inputs (simulating a case of Color Flow Mapping). To avoid an increase in the duration of the initial transients, an increase in word-length of one bit was necessary for Predictive ADC and second order DPCM.

The results are included in Table I.

D. Sensitivity

The wall thump segment in Fig. 7 and a worst-case step were used as input signals. In the former case, we recorded the increase in dynamic range (in bits) of the error signal $e[n]$ after the initial transient, with no limiting of ADC or DAC output. In the latter case we recorded the duration of the initial transient.

The results in Section VII were confirmed. For the second order DPCM dynamic range and transient duration, we found $\delta g \in [-25, 31]$ % and $\delta g \in [-0.005, 7]$ % respectively ($R_e = 5$ in the latter case). The word-length increase for first order DPCM can be approximated by the curve describing Predictive ADC word-length reduction for $f_c = 0.032 f_s$ and $\text{CNR}_{\text{rms}} = 90$ dB in Fig. 4, with $g = (a + 1)/2$. An approximation for second order DPCM is halfway between the two uppermost dashed curves in the same figure.

Offset errors less than 30Δ combined with $\delta g = \pm 2$ % had no influence on the transient durations. Concluding this section, an overall loop gain error of maximum $\delta g = \pm 2$ % will not influence the performance when $\delta R = 5$ for Predictive ADC, $\delta R = 4$ for first order DPCM, and $\delta R = 5$ for second order DPCM.

IX. Discussion

For first-order DPCM, the optimum predictor is given by $d_1 = \rho_x[1]$ (normalized lag-one autocorrelation). The prediction gain becomes $(1 - \rho_x^2[1])^{-1}$ [8]. For a word-length reduction of 5 bits (as with Predictive ADC), we get $\rho_x[1] \geq 0.9995$. From the spectral model given by f_c and CNR_{peak} for the experimental signal, we find $\hat{\rho}_x[1] = 0.9983 < 0.9995$. The maximum word-length reduction using Differential Pulse Code Modulation (DPCM), with an infinite order predictor, as given by the reciprocal of the spectral flatness in (18), is about 10 bits.

The DPCM is optimal in terms of minimizing the prediction error variance with an FIR predictor between $x[n]$ and $\hat{x}[n]$ ($\mathcal{D}(z)$ in Fig. 5). The Predictive ADC is optimal in terms of the same criterion, but it uses an IIR predictor of first degree, $\hat{\mathcal{X}}(z)/\mathcal{X}(z) = (1-a)z^{-1}/(1-az^{-1})$ (Fig. 6).

Predictive ADC is better than first order DPCM for a process with a large low-frequency clutter component. One explanation is that IIR filters have better frequency selective properties than FIR filters [17]. Also, with $d_1 \to 1$ in (15), the weighting of the error input in the numerator of (10) may be independently adjusted via the parameter a.

The Doppler signals are non-stationary, and an adaptive approach may seem appropriate. Adaptive DPCM is well known and would in this case be a natural first choice. However, we have not implemented an adaptive system, because a Predictive ADC or a DPCM which is set up to handle large low-frequency clutter, can also be used when there is less or no clutter. Reduced clutter simply implies less power in the prediction error signal (Fig. 2 and (14)) and thus a smaller required word-length. In our case a mismatch between signal and filter is not serious, as long as the clutter has low-frequency characteristic, the ADC loop is set up to handle large clutter, and the requirement on the quantization noise is constant.

An estimate of the maximum clutter frequency which corresponds in time to the maximum CNR_{peak}, is 102 Hz. This increases the estimated word-length reduction for Predictive ADC by 0.5 bit. It agrees with Fig. 8, which has a minimum of 5.5 bits ('△').

Equal loading factors for the loop input and error signal were assumed in (12). For the wall thump, $\lambda_x = 3.8$ and $4 < \lambda_e < 4.5$, depending on filter parameter a. Also, the quantization noise, $e[n] - e_q[n]$, was checked for whiteness in its power density spectrum, and the histogram indicated a roughly uniform probability density distribution.

X. Conclusion

We have completed a rigorous analysis of a Predictive ADC based on a first order recursive prediction error filter, by exploiting the characteristics of Doppler ultrasound echo signals. The Predictive ADC was compared with first and second order DPCM.

Estimates of word-length reduction, based on a reduction in dynamic range through a first order recursive prediction error filter, depend on the filter parameter, clutter bandwidth and clutter-to-noise ratio. For large clutter-to-noise ratios, the word-length reduction increases as the clutter bandwidth decreases. It also increases as the high-frequency boost and the low-frequency attenuation of the prediction error filter is increased.

For clutter-to-noise ratios above a threshold, the word-length reduction saturates for Predictive ADC. For a signal with a larger instantaneous dynamic range than our experimental signal (62 dB), the reduction in the number of bits per sample will remain at five, for the same maximum clutter frequency.

Negative values of the Predictive ADC filter parameter give better results than positive values because an extra attenuation of the large low-frequency clutter power in the ADC error input signal is achieved at the cost of an increase in the small high-frequency power. This contributes to whitening of the

error signal. The overall Predictive ADC transfer function is equal to unity, and this trade-off is not reflected.

A ranking of the three loops depends on their context. For long input signals with a large dynamic range, second order DPCM (6 bits reduction) performs better than Predictive ADC (5 bits reduction) and first order DPCM (4 bits reduction). An amplitude resolution of 16 bits at a sampling frequency of 1 MHz is thus possible with an ADC of 10 bits in a closed loop.

For short signal segments (high spatial resolution Color Flow Mapping), the initial transients must be kept short, thus minimizing the information loss prior to estimation of blood velocity. Including the effects of overall component gain errors within ± 2 %, we found that the bit reductions, in the above order, were 5, 4 and 4, with corresponding transient durations of 2, 1 and 1 sample(s). The two first order approaches may be preferable because only the first sample is corrupted.

A. Word-length reduction

From (9) and $\omega = 2\pi f T$,

$$\int \frac{1}{T^2} |B(f)|^2 \, df = \frac{2}{\pi T} \int \frac{\sin^2 \frac{\omega}{2} d\omega}{1 + a^2 - 2a \cos \omega}.$$

Using $u = \tan \frac{\omega}{2}$, $-\pi < \omega < \pi$, and $a \in \langle -1, 1 \rangle$, this becomes (apart from additive constants)

$$p(\omega; a) = \begin{cases} \frac{1}{\pi T a} \left\{ \frac{\omega}{2} - \frac{1}{K} \tan^{-1} \left[K \tan \frac{\omega}{2} \right] \right\}, & a \neq 0 \\ \frac{1}{\pi T} (\omega - \sin \omega), & a = 0, \end{cases} \tag{A.1}$$

where $K = (a+1)/(a-1) < 0$. Also,

$$p(\pi; a) = \frac{1}{T(a+1)}. \tag{A.2}$$

From (14) and odd symmetry of $p(\omega\,; a)$,

$$\sigma_e^2 = 2P_c p(\omega_c; a) + 2P_w p(\pi; a). \tag{A.3}$$

Integrating the power density spectrum of the signal model,

$$\sigma_x^2 = \sigma_c^2 + \sigma_w^2 = 2 f_c P_c \left(1 + \frac{1}{\mathrm{CNR}_{\mathrm{rms}}^2} \right). \tag{A.4}$$

Using (A.1), (A.2), (A.3), (A.4) and

$$\frac{P_w}{f_c P_c} = \frac{\sigma_w^2 2 f_c}{f_c f_s \sigma_c^2} = \frac{2T}{\mathrm{CNR}_{\mathrm{rms}}^2},$$

we get

$$\frac{\sigma_e^2}{\sigma_x^2} = \begin{cases} \frac{\beta_1}{\omega_c} \tan^{-1} \left[K \tan \frac{\omega_c}{2} \right] + \beta_2, & a \neq 0 \\ 2 - \frac{2\mathrm{CNR}_{\mathrm{rms}}^2}{\mathrm{CNR}_{\mathrm{rms}}^2 + 1} \frac{\sin \omega_c}{\omega_c}, & a = 0, \end{cases} \tag{A.5}$$

where

$$\beta_1 = -\frac{2\mathrm{CNR}_{\mathrm{rms}}^2}{(\mathrm{CNR}_{\mathrm{rms}}^2 + 1) a K}, \; \beta_2 = \frac{\mathrm{CNR}_{\mathrm{rms}}^2 (a+1) + 2a}{a(a+1)(\mathrm{CNR}_{\mathrm{rms}}^2 + 1)}.$$

Assume $\mathrm{CNR}_{\mathrm{rms}}^2 (a+1) \gg 2|a|$ and $\mathrm{CNR}_{\mathrm{rms}}^2 \gg 1$. Then $\beta_2 \approx 1/a$ and

$$\frac{\sigma_e^2}{\sigma_x^2} \approx \frac{1}{a} - \frac{2}{aK\omega_c} \tan^{-1} \left[K \tan \frac{\omega_c}{2} \right], \; a \neq 0.$$

The threshold for $\mathrm{CNR}_{\mathrm{rms}}$ increases as $a \to -1$ and as $f_c \to 0$. For $a = -0.99$ and $f_c = 0.016 f_s$, there is only 1 % variability in word-length reduction for $\mathrm{CNR}_{\mathrm{rms}}$ between 65 dB and 120 dB.

B. Initialization

The ADC overload level is $e_{\mathrm{ol}}(\Delta) = \Delta(2^{R_e - 1} - 0.5)$, $\max |e_q[n]| = 2^{R_e - 1} - 1$, $e_{\max}(\Delta) = \Delta \max |e_q[n]|$, and the conventional (open-loop) ADC overload level is $x_{\mathrm{ol}}(\Delta) = \Delta(2^{R_x - 1} - 0.5)$.

With $e[n] = e_{\max}(\Delta), \; n \geq 0$, during overload, (17) yields the Predictive ADC step response and transient duration ($x_q[n] = x[0] - \Delta/2$)

$$\begin{aligned} x_q[n] &= e_{\max}(\Delta)[1 + n(1-a)], \; n \geq 0 \\ n_0 &= \left\lceil \frac{x[0] - \Delta/2 - e_{\max}(\Delta)}{(1-a) e_{\max}(\Delta)} \right\rceil. \end{aligned} \tag{B.1}$$

Choosing the coarse step size Δ_0 to avoid overload ($e_{\mathrm{ol}}(\Delta_0) \geq x_{\mathrm{ol}}(\Delta)$), and assuming $2^{R_e} \gg 1$, we have

$$\Delta_0 = \Delta \frac{2^{R_x - 1} - 0.5}{2^{R_e - 1} - 0.5} \approx \Delta 2^{\delta R}. \tag{B.2}$$

With $\Delta_0/2$ for $x[0]$ in (B.1) (worst case), and using (B.2), $e_{\max}(\Delta)$ and $2^{R_e} \gg 2$, we get

$$n_0 \approx \left\lceil \frac{2^{R_x - 2R_e} - 1 + 2^{-R_e}}{1 - a} \right\rceil + 1$$

for Predictive ADC and first order DPCM ($a = 0$).

C. Sensitivity

With gain factor g, the pole in $\mathcal{B}(z)$ for Predictive ADC is $1 - g(1-a)$. An analysis of dynamic range with gain error is available from (A.5) and (12). An increase in 0.5 bit occurs for $a = -0.95$ and $g \approx 0.65$. Stability requires $g \geq 1.025$. Thus, $\delta g = 1 - g \in [-35, 2]$ % is tolerable. For first order DPCM ($a = 0$), $\delta g \in [-30, 100]$ %.

From Table I, $n_0 = 1$ in all cases but second order DPCM with $R_e = 5$. We only need the condition for $n_0 \leq 2$ in these cases, $|e[1]| \leq e_{\mathrm{ol}}(\Delta)$, where $e[1] = x[1] - g x_0$, and $x_0 = x[0] \pm \Delta_0/2$. For the two Predictive ADC cases with $x[0] \approx 2 x_{\mathrm{ol}}(\Delta)/3$, we find, using (B.2), that $|g - 1| \leq 2$ % and 7 % respectively. First and second ($R_e = 6$) order DPCM require $|g - 1| \leq 7$ % ($R_e = 7$).

References

[1] W. J. Bommer and L. Miller, "Real-time two-dimensional color-flow Doppler: Enhanced Doppler flow imaging in the diagnosis of cardiovascular disease," *Am. J. Cardiol.*, vol. 49, p. 944, 1982.

[2] M. Brandestini, *Signalverarbeitung in perkutanen Ultraschall Doppler Blutfluss Messgeräten*. PhD thesis, Eidgenossischen Technischen Hochschule Zürich, Zürich, Switzerland, 1976.

[3] A. P. G. Hoeks, R. S. Reneman, and P. A. Peronneau, "A multigate pulsed Doppler system with serial data processing," *IEEE Trans. Sonics Ultrason.*, vol. 28, pp. 242–247, July 1981.

[4] A. P. G. Hoeks, *On the Development of a Multi-gate Pulsed Doppler System with Serial Data-processing*. PhD thesis, University of Maastricht, Maastricht, The Netherlands, 1982.

[5] L. Hatle and B. Angelsen, *Doppler Ultrasound in Cardiology*. Philadelphia, USA: Lea & Febiger, second ed., 1985.

[6] F. Jay, ed., *IEEE Standard Dictionary of Electrical and Electronics Terms*, pp. 574–575. New York, USA: IEEE, Inc. & Wiley-Interscience, John Wiley & Sons, third ed., 1984.
[7] M. I. Skolnik, ed., *Introduction to Radar*. New York, USA: McGraw-Hill Publishing Company, 2 ed., 1980.
[8] N. S. Jayant and P. Noll, *Digital Coding of Waveforms*. Prentice-Hall Signal Processing Series, New Jersey, USA: Prentice-Hall, Inc., 1984.
[9] M. Hauser, "Principles of oversampling A/D conversion," *J. Audio Eng. Soc.*, vol. 39, pp. 3–26, Jan.,Feb. 1991.
[10] Analog Devices, Inc., *Data Conversion Products Databook 1989/90*, July 1989.
[11] Y. Nejime, M. Hotta, and S. Ueda, "An 8-bit ADC with over-Nyquist input at 300-Ms/s conversion rate," *IEEE J. Solid-State Circuits*, vol. 26, pp. 1302–1308, Sept. 1991.
[12] S. H. Lewis, H. S. Fetterman, G. F. Gross, Jr., R. Ramachandran, and T. R. Viswanathan, "A 10-b 20-Msample/s analog-to-digital converter," *IEEE J. Solid-State Circuits*, vol. 27, pp. 351–358, Mar. 1992.
[13] B. P. Brant and B. A. Wooley, "A 50-MHz multibit sigma-delta modulator for 12-b 2-MHz A/D conversion," *IEEE J. Solid-State Circuits*, vol. 26, pp. 1746–1756, 1991.
[14] M. Brandestini, "Topoflow – a digital full range Doppler velocity meter," *IEEE Trans. Sonics Ultrason.*, vol. 25, pp. 287–293, Sept. 1978.
[15] M. A. Brandestini and F. K. Forster, "Blood flow imaging using a discrete-time frequency meter," in *Proc. Ultrason. Symp.*, (Cherry Hill, New Jersey, USA), pp. 348–352, IEEE, Sept. 1978.
[16] L. R. Rabiner and R. W. Schafer, *Digital Processing of Speech Signals*. Prentice-Hall, Inc., 1978.
[17] A. V. Oppenheim and R. W. Schafer, *Digital Signal Processing*. Prentice-Hall, Inc., 1975.
[18] S. L. Marple Jr., *Digital Spectral Analysis with Applications*. Prentice-Hall Signal Processing Series, Prentice-Hall, Inc., 1987.
[19] S. M. Kay, *Modern Spectral Estimation – Theory & Application*. Prentice-Hall Signal Processing Series, Prentice-Hall, Inc., 1988.

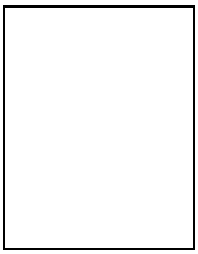

Svein Bøe received the M.S. degree from the University of Oslo in 1987. He has been a research fellow at the University of Oslo, Norway, and has collaborated with Vingmed Sound A.S., Norway, on Doppler ultrasound signal processing. His interests are digital signal processing, spectral estimation, medical imaging, and multirate signal processing.

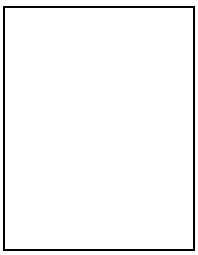

Kjell Kristoffersen was born in Karmøy, Norway, in 1952. He received the M.S. and Dr.Techn. degrees from the Norwegian Institute of Technology, Trondheim, Norway, in 1978 and 1986, respectively. From 1978 to 1984, he worked with research and development in several areas of process identification and Doppler ultrasound at the Division of Automatic Control, SINTEF, Trondheim, Norway. Since 1984 he has been involved with development of medical ultrasound imaging systems at Vingmed Sound A.S., where he currently holds the position of Director of Research. His research interests include signal processing with application to medical imaging and noninvasive diagnosis.